SPACE-TIME VARIABILITY OF SUBCANOPY HORIZONTAL ADVECTION IN MODERATELY COMPLEX TERRAIN

Christoph K. Thomas[1*]

[1] College of Oceanic and Atmospheric Sciences, Oregon State University, Corvallis OR, USA

1   Introduction

Over the past few decades many micrometeorological studies have focused on the contribution of advective components to the energy and mass budgets to quantify land surface-atmosphere exchange, particularly for carbon dioxide, sensible, and latent heat. Most studies were conducted in tall canopies, where the above-canopy flow is often decoupled from the flow inside the canopy (e.g. Thomas and Foken, 2007), and that are often located in complex terrain. In general, results were ambiguous with regard to the hypothesis that including terms other than the turbulent vertical flux and the change in storage term may yield better budget closures. However, some studies demonstrated that the inclusion of advective fluxes improves budgets at night when radiative cooling often leads to stable stratification suppressing turbulent diffusion. Patterns in daytime advection were less consistent and showed large scatter. Despite these advances, little attention has been given to the space-time variability of the wind field, scalar gradients, and resulting advective components in plant canopies. The lack of knowledge of the space-time variability of scalar gradients in the canopy has been identified as one of the most likely causes hindering significant progress in the discussion of advective fluxes (Aubinet et al., 2010).

In this study, the analysis of spatial observations from a sensor network operated over a period of several months in the subcanopy of a forest with a very dense overstory was directed toward the following objectives:

- Analyze the variability of the space-time structure of the subcanopy wind and temperature fields, as well as the resulting horizontal advection of sensible heat.

- Evaluate the impact of sensor network geometry and method of analysis on the magnitude and variability of horizontal advective components.

[*]Corresponding author: Christoph K. Thomas, College of Oceanic and Atmospheric Sciences, Biomicrometeorology Group, Oregon State University, 104 COAS Admin Bldg, Corvallis, OR 97331, USA; Phone: +1(541) 737 7690; Email: chthomas@coas.oregonstate.edu
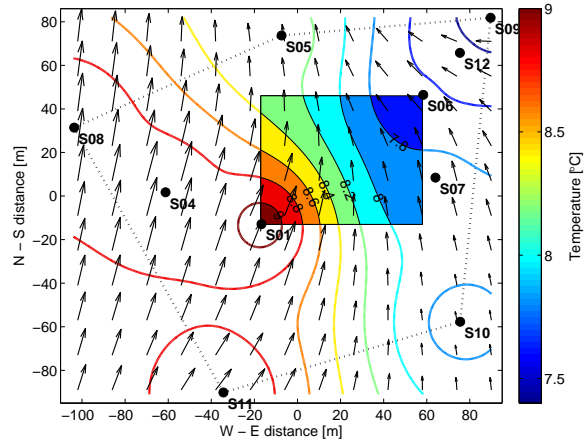
Figure 1: Configuration of the sensor network consisting of ten stations (S01 to S12) and sampling domain (dotted lines). Also shown is the average (64 min mode) structure of the air temperature (isolines) and the wind field (vectors) sampled at 1 m agl. Spatially discrete sampled winds and air temperatures were interpolated using the inverse square weighting method. The filled rectangle represents an example of the subdomain of the station pair S01-S06 when determining the variability of spatial gradients and horizontal advection.

2   Data and methods

Data were collected with a sensor network in a 33-year-old mature Douglas-Fir forest located in the coast range of western Oregon, U.S.A. (44.646N latitude, 123.551W longitude, 310 m elevation; Thomas et al., 2008) during the period from 28 Aug (DOY 241) through 17 Dec (DOY 352) 2008. The overstory is very homogeneous and has an average height of 26 m; the plant area index (PAI) is 9.4 $m^2 m^{-2}$. The closure of the overstory is very high creating only small gaps that permit sunlight to enter the subcanopy space. Concurrent observations of shortwave radiation in the subcanopy next to the network stations yielded that irradiances were typically $\leq 100\ W m^{-2}$ even under clear-sky conditions during the summer months.

The sensor network consisted of ten stations each comprised of one 2-D sonic anemometer (Model WAS425A, Vaisala Inc.) and one naturally ventilated

air temperature sensor (external thermistor, Model HOBO H8 Pro, Onset Computer) in a radiation shield mounted at 1 m agl on a guyed tripod. Running $10s$-averages of the raw measurements of the horizontal wind speed components (u, v) internally sampled at 1 Hz were interrogated and stored by a single data logger (Model CR1000, Campbell Sci.) using the SDI-12 interface for the entire network. Temperature data (T) were recorded and stored in the onboard memory of each sensor at a sampling interval of 2 min. As the calculation of spatial gradients is sensitive to systematic and random instrument-specific errors, all sensors were carefully cross-calibrated in a laboratory environment and field tests prior to field deployment. The precision of the wind speed measurements was determined to be ± 0.10 ms^{-2}, that of the thermistors ± 0.05 K, and that of the thermistors in the naturally ventilated radiation shields ± 0.10 K.

Data from all sensors and stations were orthogonally decomposed into the local multiresolution basis set (e.g. Howell and Mahrt, 1997) which decomposes a signal into unweighted averages over subrecords of dyadic width (2^n). The resulting multiresolution time scales were 64, 32, 16, 8, 4, 2, and 1 min. Temperature data were analyzed only for time scales ≥ 4 min because of the large time constant of the thermistor low-pass filtering the signal. In a first step, the stochastic analysis of the network data was performed using various measures of time and space variability applied separately to each multiresolution time scale (m) including the two-point correlation coefficients (R_x) following Mahrt et al. (2009). In a second step, the sampled variable fields $u_m(x, y)$, $v_m(x, y)$, $T_m(x, y)$ containing all stations were then non-linearly interpolated using the inverse square weighting method to a resolution of 0.5 m in both longitudinal (y) and latitudinal (x) directions while recognizing that only motions on horizontal scales greater than the minimum station spacing were resolved. The horizontal temperature gradients between two stations (Γ_x, Γ_y) were calculated by fitting a plane to the interpolated values of the subdomain defined by the stations' locations (see the filled rectangle in Fig. 1 for an example). Subsequently, the temporal average TAG, the time-dependent variance TVG of the temperature gradients were computed. The horizontal advection $\Psi_{ij}(r)$ between two stations indexed i and j for each subrecord was computed by combing the spatial temperature gradients with the interpolated wind components averaged over the subdomain leading to

$$\Psi_{ij}(r) = \int \int \langle (u_{ij}) \Gamma_{x,ij}(r) + \langle v_{ij} \rangle \Gamma_{y,ij}(r)) \, dxdy,$$

(1)

where r is the separation distance. In a last step, the temporal average $TAA_{ij}(r)$ of the horizontal advection was computed in a fashion analogous to those of the temperature gradients.

3   Results & Discussion

Results were generally partitioned into diurnal periods differentiating between night, transition period, and daytime based on geometrically calculated azimuth and zenith angles at the site's location. Transition period was defined as the 64 min subrecord in which sunrise or sunset occurred.

3.1   Wind and temperature fields

The correlation of the flow $R_{uv,ij}$ was a function of separation distance between stations independent of time scale (Fig. 2). The fast decay of $R_{uv,ij}$ with separation distance, which was particularly visible for short time scales, demonstrates that the underlying motions are short-lived and small in spatial extent. In contrast, larger-scale transient motions moving at high velocities would maintain a high spatial correlation at the shorter time scales. The scatter of the correlation $R_{uv,ij}$ for a specific separation distance was largest for the longest time scale (64 min mode containing the time-averaged mean), which suggests that each station has a location-specific wind microclimate. This wind microclimate is likely to depend on the presence of individual flow obstacles such as individual bushes, tree boles, and local topography leading to systematic deviations from the domain-averaged flow field.

The analysis of the space-time structure of the temperatures revealed some similarities, but also important differences compared to that of the velocities. The two-point temporal correlation of the temperature $R_{T,ij}$ behaved similarly to that of the velocity field with the exception of the largest 64-min mode, which showed no decorrelation even for the largest spatial scales (Fig. 2). This independence of spatial scale can be explained by the diurnal cycle of air temperature forced by the solar heating during the daylight hours and the radiative cooling at night. The perfect correlation independent of location indicates that all stations were consistently participating in this diurnal oscillation, while effects of systematic decoupling, e.g. through the presence of cold air pools, were negligible or absent at this site. The increased scatter in correlation of temperature signals detected for the shortest scales (4 min) at night was caused by data collected at station S01. The temperature records at this station
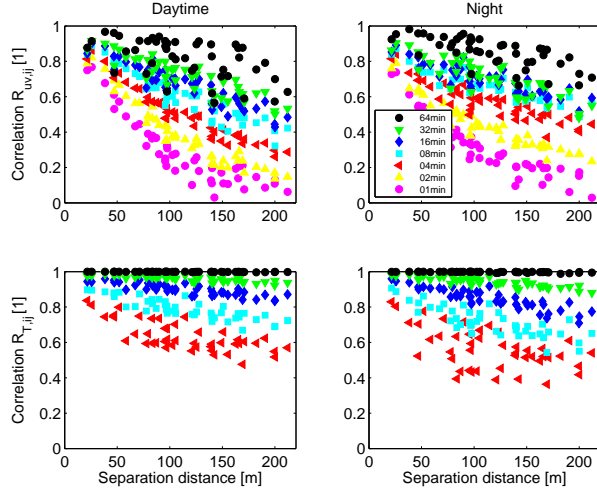
Figure 2: Two-point correlation of the wind ($R_{uv,ij}$) and temperature ($R_{T,ij}$) versus separation distance between stations as a function of time scale (multi-resolution mode) for all 45 station pairs over the entire dataset.

were often decoupled from the spatial average of the rest of the domain.

3.2 Temperature gradients and horizontal advection

The spatial temperature gradients were more systematic at night than during the day, and decreased with increasing station spacing (Fig. 3). This result is in agreement with the findings of the higher daytime variability of the bulk stochastic measures in the previous subsection. For the nighttime case, the time-averaged gradients TAG_{ij} were found to become independent of spatial scale only for separation distances exceeding 100 to 150 m. Gradients during the day showed a large scatter with frequent changes in sign and only a weak dependence on separation distance, and did not converge to a consistent value, even for the largest spatial scales of the domain. Differences between time scales were much smaller than those found between different paired stations, confirming the importance of stations' position and spatial variability within the domain. The time-dependent variability of the spatial temperature gradients TVG_{ij} decayed with increasing station spacing in a non-linear fashion, but also failed to converge to a constant value on the spatial scales of the domain.

In order to evaluate the impact of the network configuration and method of analysis as one of the study's objectives, the computation of spatial gradients was repeated based on a subset of the full domain. This
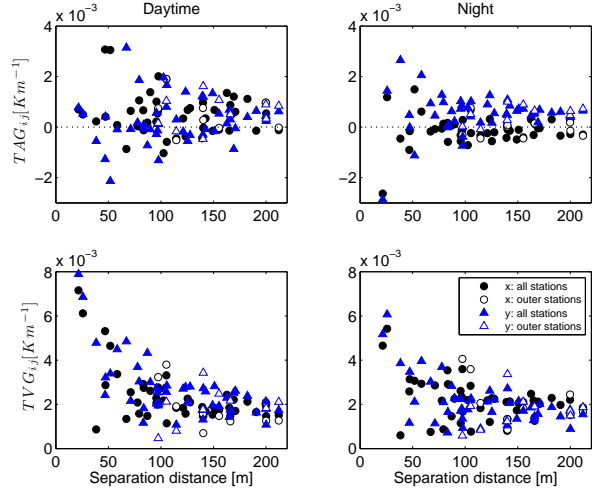
Figure 3: Time average (TAG_{ij}) and time-dependent variability (TVG_{ij}) of spatial temperature gradients for the 32 min time scale (multiresolution mode) as a function of station spacing over the entire length of the dataset. Measures were evaluated for two different network configurations (see Fig. 1): all ten stations (S01-S12, filled symbols), and outer stations only (S08, S05, S09, S10, S11, open symbols).

subset used observations from the outer stations only (S08, S05, S09, S10, S11, see Fig. 1) and allowed for testing the common assumption of linear gradients within a domain (e.g. Moderow et al., 2007). In general, the temporal averages and the variability of the temperature gradients computed from this subset exceeded those derived from the full domain indicating that at least for this site, it is insufficient to approximate spatial gradients linearly (Fig. 3).

In contrast to the temporal variability of spatial gradients, the scatter of the resulting time-averaged horizontal advection of sensible heat ($TAA_{xy,ij}$) was smallest for the smallest spatial scales, then increased until approximately the 100 m scale, and then remained large for all lager scales (Fig. 4). This finding suggests a high degree of spatial non-linearity in the observed horizontal advection that may result from the fundamental differences in space-time structure of the wind and temperature fields. The variability of the advective fluxes with spatial scales was similar for day- and nighttime data, while the daytime estimates showed a more consistent, negative sign. Generally, the smallest spatial scales yielded horizontal advective fluxes approximately equal to zero, and the magnitude increased with increasing spatial scale. $TAA_{xy,ij}$ was found to be systematically negative only for spatial scales exceeding approximately 150 to 180 m, which is close to the upper limit of scales resolved by the net-
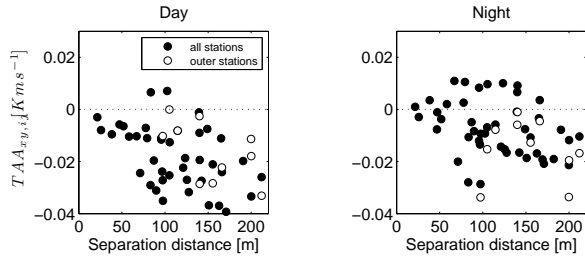
Figure 4: Total resultant ($TAA_{xy,ij}$, bottom) temporal average of the horizontal advection of sensible heat for the 32 min mode as a function of station separation distance. Measures were evaluated for two different configurations: all ten stations (S01-S12), and outer stations only (S08, S05, S09, S10, S11).

work. Based on these findings, the horizontal size of the control volume used for an evaluation of the energy balance must not be smaller than 180 m to yield results with a systematic sign for the contribution of horizontal advection, at least for this site.

4   Conclusions

One arrives at the following conclusions with regard to the two objectives of this study:

- The computation of the horizontal advection of sensible heat is inherently aggravated by this mismatch in space-time structure and suffers from a strong spatial non-linearity. This finding may provide an explanation for the ambiguous results on the contribution of horizontal advection to the canopy budgets of energy and mass reported in the literature. The variability of the horizontal advection with spatial scale was particularly large for domain sizes between 70 and 150 m, commonly used in the literature. At least at this site, the advective fluxes became more systematic in sign only for sizes of the control volume exceeding 180 m, while the variability of horizontal advection in magnitude remained large even at these large spatial scales.

- The placement of stations within a domain, as well as the overall density (number) of stations of a network profoundly impact the calculated spatial gradients and the estimates of horizontal advection. A larger number of stations facilitates a better resolution of the non-linear spatial gradients of the wind and temperature fields, while no recommendation can be made for an optimal number of stations based on the existing data. Incorporating elements of the canopy and the terrain that contribute to within-domain heterogeneity at least provides a framework to interpret spatial gradients and advective fluxes in the context of the site's heterogeneity and space-time variability. Spatial temperature gradients and advective fluxes were also sensitive to the spatial interpolation algorithm of the velocity and temperature fields, which may provide perspective for an alternate interpretation of existing studies.

References

Aubinet, M., C. Feigenwinter, B. Heinesch, C. Bernhofer, E. Canepa, A. Lindroth, L. Montagnani, C. Rebmann, P. Sedlak, and E. van Gorsel, 2010: Direct advection measurements do not help to solve the night-time co2 closure problem: Evidence from three different forests. *Agricultural and Forest Meteorology*, **150**, 655–664.

Howell, J. F. and L. Mahrt, 1997: Multiresolution flux decomposition. *Boundary-Layer Meteorology*, **83**, 117–137.

Mahrt, L., C. Thomas, and J. Prueger, 2009: Space-time structure of mesoscale modes in the stable boundary layer. *Quarterly Journal of the Royal Meteorological Society*, **135**, 67–75.

Moderow, U., C. Feigenwinter, and C. Bernhofer, 2007: Estimating the components of the sensible heat budget of a tall forest canopy in complex terrain. *Boundary-Layer Meteorology*, **123**, 99–120.

Thomas, C. and T. Foken, 2007: Flux contribution of coherent structures and its implications for the exchange of energy and matter in a tall spruce canopy. *Boundary-Layer Meteorology*, **123**, 317–337.

Thomas, C., J. G. Martin, M. Goeckede, M. B. Siqueira, T. Foken, B. E. Law, H. W. Loescher, and G. Katul, 2008: Estimating daytime subcanopy respiration from conditional sampling methods applied to multi-scalar high frequency turbulence time series. *Agricultural and Forest Meteorology*, **148**, 1210–1229.